# Double acoustic microresonator quartz-enhanced photoacoustic spectroscopy

**Lei Dong,[1,*] Hongpeng Wu,[1] Huadan Zheng,[1] Yanyan Liu,[1] Xiaoli Liu,[1] Wenzhe Jiang,[2] Lei Zhang,[1] Weiguang Ma,[1] Wei Ren,[2] Wangbao Yin,[1] Suotang Jia,[1] and Frank K. Tittel[2]**

[1]*State Key Laboratory of Quantum Optics and Quantum Optics Devices, Institute of Laser Spectroscopy, Shanxi University, Taiyuan 030006, China*

[2]*Department of Electrical and Computer Engineering, Rice University, 6100 Main Street, Houston, Texas 77005, USA*

**Corresponding author: donglei@sxu.edu.cn*

Received February 20, 2014; accepted March 16, 2014;
posted March 20, 2014 (Doc. ID 206769); published April 14, 2014

Quartz-enhanced photoacoustic spectroscopy (QEPAS) based on double acoustic microresonators (AmRs) is developed and experimentally investigated. The double AmR spectrophone configuration exhibits a strong acoustic coupling between the AmR and the quartz tuning fork, which results in a ~5 ms fast response time. Moreover, the double AmRs provide two independent detection channels that allow optical signal addition or cancellation from different optical wavelengths and facilitate rapid multigas sensing measurements, thereby avoiding laser beam combination. © 2014 Optical Society of America

*OCIS codes:* (280.3420) Laser sensors; (300.6430) Spectroscopy, photothermal; (300.6260) Spectroscopy, diode lasers.

http://dx.doi.org/10.1364/OL.39.002479

Photoacoustic spectroscopy (PAS) is one of the most sensitive techniques to measure low gas concentrations at atmospheric pressure, due to its zero-background nature, which means that no PAS signal is produced in the absence of an absorbing species [1]. The two most outstanding features of the PAS technique are that it is excitation wavelength independent and its sensitivity is proportional to incident laser power. The first advantage allows the same PAS-based detector to be used with any type of laser and at any wavelength, from ultraviolet to mid-infrared, with identical performances. Thus, a different wavelength-based multigas photoacoustic sensor can be realized in one instrument [2]. The second advantage makes the PAS-based detectors benefit from the development of high-power semiconductor lasers with high wall plug efficiency [3,4] or from the enhanced excitation power [5].

Quartz-enhanced photoacoustic spectroscopy (QEPAS) is a variant of PAS, in which a commercially available high-$Q$ quartz tuning fork (QTF) is employed as a resonant acoustic transducer instead of the conventional wideband microphone [6–8]. It combines the main characteristics of PAS with the benefits of a QTF, providing a robust, ultracompact, and cost-effective spectrophone. Thus, compared with the size of the conventional photoacoustic cell, typically starting from ~10 $cm^3$ [1], the dimensions of the QEPAS-based acoustic detection module is ~2 $cm^3$ [9], which matches the laser source in size, but an accuracy of the optical collimation is required from mms down to μms. As a result, it is a significant experimental challenge to couple effectively two different wavelength laser beams into a QEPAS spectrophone via beam combination due to the aberration of optical elements, as for example, in a QEPAS-based two-gas system or when using a modulation cancellation method [10]. The use of optical fiber coupling can simplify collimation. Fiber collimating based multigas QEPAS sensors and mid-infrared QEPAS sensors have been reported [11–13]. However, the transmission characteristics of optical fibers are wavelength dependent and cannot accomplish beam combination of two lasers with a large wavelength difference.

QEPAS spectrophones have an inherently high $Q$ factor, resulting in long accumulation times of the acoustic energy. Therefore, it is not practical to configure a QEPAS-based sensor for spectral scans of an absorption line. Instead, the laser wavelength must be locked to the target absorption line center. Kosterev *et al.* reported a rapid QEPAS sensor for the measurement of wide spectral lines, however with a response time of 20 ms [14].

In this Letter, we report a novel configuration of the QEPAS spectrophone and demonstrate for the first time the performance of two optical signal additions and multigas rapid measurements by use of such a spectrophone. The new spectrophone configuration employs two acoustic microresonators (AmRs) to construct two detection channels based on the "on-beam" QEPAS approach [15,16], as depicted in Fig. 1. Each AmR is formed by two thin tubes and is coupled to the QTF via an excited sound wave in gas contained inside the AmR tubes. Two laser beams can pass the two AmRs from both sides, respectively, thereby avoiding laser beam combination.

The innovative double AmR QEPAS is based on the fact that there is a wider sensitive area on a QTF for sound wave detection due to the viscous drag caused by the presence of an AmR [17], rather than the previously reported position of 0.7 mm below opening of the QTF although it is true for a bare QTF [18]. The signal-to-noise ratio (SNR) and $Q$ factor of the "on beam"

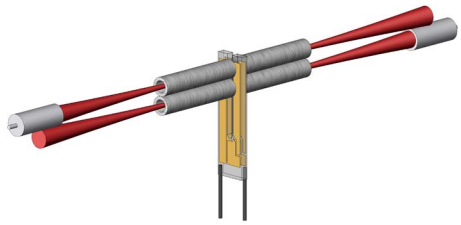

Fig. 1. Schematic of double AmR QEPAS.

 

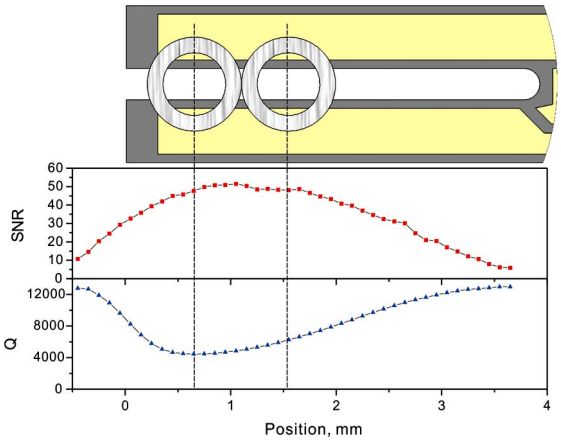


Fig. 2. SNR and $Q$ factor of an "on beam" QEPAS with an AmR as a function of the position of the AmR. The zero position is the opening of the QTF. The QTF and AmRs are scaled to position coordinate that represent the actual size and position. The AmR consists of two 4.4 mm long thin tubes with a 0.6 mm ID and a 0.9 mm OD.

QEPAS with an AmR as a function of the position are shown in the bottom part of Fig. 2. The horizontal axis represents the center position of the AmR. The flat area of SNR between 0.2 and 2 mm is sufficient to accommodate two AmRs in contact with each other, as depicted in the top part of Fig. 2.

Two different double AmR spectrophones were fabricated and numbered Double AmR #1 and #2. The gaps between the thin tubes and the QTF were 20 μm. Each double AmR spectrophone has two identical AmRs, but the AmRs' tube dimensions of the Double AmR #1 and #2 are different. The tube parameters for the top and bottom channels and measured electrical parameters are listed in Table 1. The choice of the selected tube parameters is based on the fact that 4.4 mm long tubes with 0.6 mm inner diameter (ID) were found to be optimal for the visible and near-infrared region, while the 4.0 mm long tubes with 0.84 mm ID are the best choice for the mid-infrared region in a single AmR configuration [19]. The parameters of two single AmR spectrophones using similar tubes and bare QTF are shown in Table 1 as well as two double AmR configurations. The Double AmR #1 shows a very low $Q$ factor, which implies a strong acoustic coupling between the QTF and the two AmRs, because the high-$Q$ QTF loses energy primarily via coupling to the low-$Q$ AmR oscillator. Moreover, it presents a higher resonant frequency $f_0$ than that of a bare QTF, which indicates that an additional force constant is added due to the acoustic coupling. We expect to see a lower $Q$ factor for the Double AmR #2, because the Single AmR #2 shows a lower $Q$ factor than the Single AmR #1 for the single AmR configuration, which is well known from previously reported designs [14,15]. However, the $Q$ factor of the Double AmR #2 decreases to only 1890. An explanation of this observation is that the 1.24 mm outer diameter (OD) places the two tubes centers far away from the sensitive area of the QTF, so that the acoustic coupling between the QTF and two AmRs decreases. According to classical oscillator theory, the response time $\tau$ for the vibration amplitude to decay to $1/e$ of the initial value can be calculated from $Q/\pi f_0$ [14]. The calculated $\tau$ values for all configurations are listed in Table 1. For the single AmR configuration, the Single AmR #2 has a faster response time of ~20 ms, which is in agreement with [14], while for the double AmR configuration, the Double AmR #1 exhibits a faster response time of ~6 ms due to a low $Q$ factor caused by strong coupling. The response time is 23 times faster than that of the bare QTF.

A schematic of the experimental setup is shown in Fig. 3 to demonstrate the performance of the double AmR spectrophone. A distributed feedback (DFB) laser (DL1) with a wavelength of 1368.7 nm was mounted onto a driver board (Driver 1). The driver board can control the laser temperature and supply 0–200 mA or 0–400 mA current to the DL1 depending on the external input voltage of 0–5 V and current range settings on the board. The function generator 1 (Agilent Model 33210A) was used to generate a sine signal modulation of the DL1 wavelength at a frequency $f = f_0/2$. A second DFB laser (DL2) with the same wavelength was mounted onto the Driver 2, which is identical to the Driver 1. To maintain the modulation phase relationship between the two lasers, the function generator 2 (Agilent Model 33210A) was set to the burst mode of the one-cycle sine wave triggered by the sync signal from the function generator 1. Thus, it is possible to generate the same frequency sine wave whose amplitude and phase can be adjusted independently. The sine wave was applied to modulate the DL2 wavelength. A double channel arbitrary waveform generator (AFG) (Tektronix Model AFG3102) generated two pulse ramp waves, which were superimposed with the modulation signals via two electrical adders and then applied to the DL1 and DL2, respectively, for laser

**Table 1. Intercomparison of Different QEPAS Spectrophone Configurations**

| | | Tube Parameter (mm) | | | | | | | Response Time $\tau$ (ms) | |
|---|---|---|---|---|---|---|---|---|---|---|
| Configuration | Channel | Inner diameter | Outer diameter | Length | Resonant frequency $f_0$ (Hz) | $Q$ Factor | Equivalent resistance $R$ (k ohm) | NNEA ($\mathrm{cm^{-1}\,W/\sqrt{Hz}}$) | Cal. | Meas. |
| Double AmR #1 | Top | 0.6 | 0.9 | 4.4 | 32 841 | 594 | 1 991 | $7.8\times10^{-9}$ | 5.8 | 5.0 |
| | Bottom | 0.6 | 0.9 | 4.4 | | | | $8.1\times10^{-9}$ | | |
| Double AmR #2 | Top | 0.84 | 1.24 | 4.0 | 32 747 | 1 890 | 647 | $4.5\times10^{-9}$ | 18.4 | 18.1 |
| | Bottom | 0.84 | 1.24 | 4.0 | | | | $6.6\times10^{-9}$ | | |
| Single AmR #1 | | 0.6 | 0.9 | 4.4 | 32 742 | 4 109 | 292 | $1.8\times10^{-9}$ | 40.0 | 42.3 |
| Single AmR #2 | | 0.84 | 1.24 | 4.0 | 32 758 | 2 160 | 564 | $2.2\times10^{-9}$ | 21.0 | 20.1 |
| Bare QTF | | | | | 32 752 | 13 466 | 87 | $5.2\times10^{-8}$ | 130.9 | 136.3 |

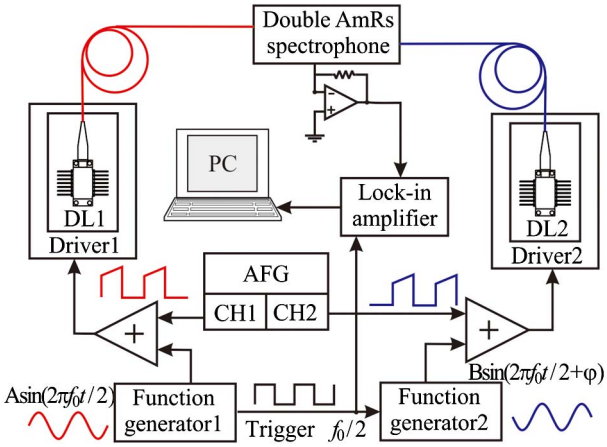


Fig. 3. Experimental setup: DL, diode laser; AFG, Tektronix arbitrary waveform generator; PC, personal computer.

wavelength scanning. The two pulse ramp signals maintained their specific phase relations. The laser beams from the DL1 and DL2 were focused into the top and bottom detection channels of the double AmR spectrophone, respectively, via two fiber-coupled focusers (OZ optics Model LPF-01). The piezoelectric signal of the QTF was sent to a lock-in amplifier (LIA) (Stanford Model SR830) via a customized preamplifier. A computer was used to communicate with the LIA and to acquire the double AmR QEPAS data.

The detection sensitivities of the two double AmR spectrophones were assessed. An $H_2O$ absorption line at 7296.65 $cm^{-1}$ with a line intensity of $8.501 \times 10^{-25}$ $cm^{-1}/(mol\,cm^{-2})$ was chosen as the target, as shown in Fig. 4. There are two weaker neighbor lines at 7296.85 $cm^{-1}$ and 7296.87 $cm^{-1}$ which merge together at atmospheric pressure. In order to reach the target wavelength, the temperature of the DL1 was set to 29.55°C with an output power of ~19 mW, while the temperature of the DL2 was set to 36.00°C with an output power of ~13 mW due to the different characteristics of these two lasers. The time constant of the LIA was 300 ms corresponding to a detection bandwidth of

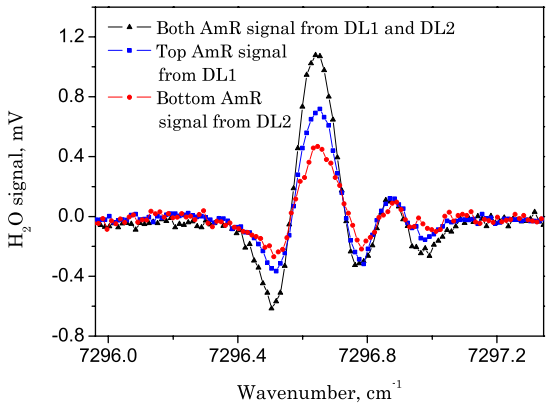


Fig. 4. Spectral data of 4540 ppm $H_2O$ acquired with the Double AmR #1. Rectangle, absorption spectrum from the top channel when the bottom channel is idle; circle, absorption spectrum from the bottom channel when the top channel is idle; triangle, absorption spectrum when both channels operate simultaneously.

$\Delta f = 0.833$ Hz. The measured rms voltage noise $(\langle V_N^2 \rangle)^{1/2}$ at the preamplifier was 22.5 μV for the Double AmR #1 and 35.2 μV for the Double AmR #2, which are in agreement with the theoretical QTF thermal noise, 20.0 and 33.0 μV, respectively, according to the expression $(\langle V_N^2 \rangle)^{1/2} = 2^{-1/2} R_{fb}\ (4\ kB\,T\Delta f/R)^{1/2}$, where $T$, $R_{fb}$, and $R$ are the temperature, the 10 MΩ amplifier feedback resistor, and the equivalent QTF resistance [15]. Hence the noise characteristics of the double AmR configuration still agree with the single AmR configuration, and no additional noise is introduced. The currents of two lasers were scanned, respectively, from 100 to 140 mA, in 120 steps and 1 s time interval. This corresponds to a wavenumber range from 7295.96 $cm^{-1}$ to 7297.57 $cm^{-1}$. The spectrophone was filled with ambient air containing 4540 ppm water vapor at atmospheric pressure. This provided a peak absorption coefficient $\alpha = 1.9 \times 10^{-5}$ $cm^{-1}$ at 7296.65 $cm^{-1}$. The normalized noise equivalent absorption coefficients (NNEAs) of all AmR configurations resulting in a SNR of 1 at a 1 W laser power level and 1 Hz detection bandwidth are reported in Table 1. The NNEAs of the single AmR configurations are generally lower than that of the double AmR configuration. In the case of two double AmR configurations, the Double AmR #2 with a higher $Q$ factor has a lower NNEA. This is due to the fact that with the stronger coupling of the Double AmR #1 between QTF and two AmRs, a channel of energy dissipation is established between the top and bottom AmRs and the QTF. When the top AmR operates alone, the QTF loses energy via coupling to the bottom AmR and vice versa. The channel of energy dissipation for the Double AmR #2 is less effective due to the weak coupling. Therefore, the fast dynamic response of the double AmR configuration comes at the cost of sensitivity ($Q$ factor). The configuration provides an additional detection channel, which makes it feasible for the double AmR configuration to be used in optical signal addition or cancellation as well as for rapid multigas sensing measurements, thereby avoiding the need of implementing a more complex laser beam combination technique.

An example of energy combination of the two lasers, DL1 and DL2, is shown in Fig. 4. The Double AmR #1 was employed here. The phases of the LIA and function generator 2 were adjusted, respectively, so that all the signals from the top and bottom channels remain on the in-phase component (X) of the LIA. The AFG was set synchronously to scan both laser wavelengths. The curve indicated by triangle markers in Fig. 4 resulted from the superposition of the two signals. The peak value of 1.1 mV at 7296.65 $cm^{-1}$ from the synchronous scanning is equal to the sum of the top AmR peak value of 0.71 mV and the bottom AmR peak value of 0.47 mV from the single channel scanning. These values indicate that the combined action of the two AmRs is based on a linear superposition effect.

In order to verify the fast dynamic characteristics of the Double AmR #1, the time constant of the LIA was set to 1 ms, which yields a detection bandwidth of 250 Hz. Thus, the response speed of the system is determined by the bandwidth of the QTF itself since the LIA bandwidth is ~3 times more than the QTF equivalent noise bandwidth (ENBW $= \pi f_0/2Q = 86.8$ Hz) [14]. A

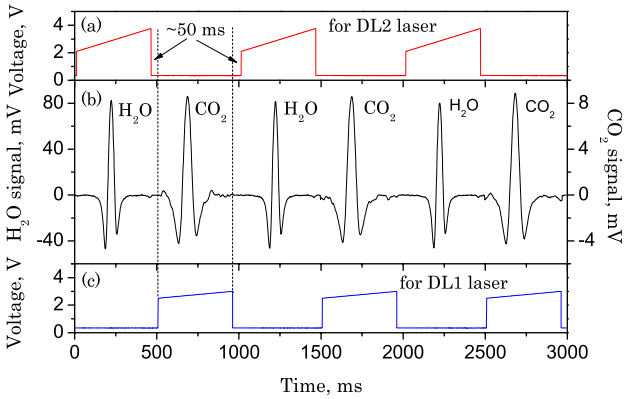


Fig. 5. Two-gas rapid-scan measurements using a double AmR configuration. Top, wavelength ramp signal for a diode laser targeting $H_2O$. Bottom, wavelength ramp signal for diode laser targeting $CO_2$. Middle, alternative appearance of $H_2O$ and $CO_2$ 2f QEPAS spectra.

$H_2O$ absorption line at 7306.75 $cm^{-1}$ with a strong line intensity of $1.8 \times 10^{-20}$ $cm^{-1}/(mol\,cm^{-2})$ was chosen to observe the clear signal. The temperature of the DL2 was set to 15.62°C, and the current was scanned at a 10 Hz rate from 78 to 145 mA, which corresponds to ~27 $cm^{-1}/s$ scan rate. A spectral line with an exponentially decaying tail was observed, as depicted in Fig. 4 in [14], which results in an amplitude decrease and an asymmetric waveform. The measured decay time of $5 \pm 0.5$ ms from the exponential fit is in a good agreement with the calculated $\tau = 5.8$ ms. The measured $\tau$ values for all configurations are also listed in Table 1 for comparison.

To demonstrate the capability of double AmR QEPAS for two-gas rapid spectral measurements, a DFB laser with a wavelength of 1572.0 nm replaced the DL1 $H_2O$ laser. A $CO_2$ absorption line at 6361.25 $cm^{-1}$ with a line intensity of $1.732 \times 10^{-23}$ $cm^{-1}/(mol\,cm^{-2})$ was chosen as detection target for the DL1. The temperature of the DL1 was set to 30.5°C with an output power of ~32 mW, and the current was scanned from 200 to 240 mA, corresponding to a wavenumber range from 6360.66 $cm^{-1}$ to 6361.83 $cm^{-1}$. The AFG generated two reciprocal pulse ramp signals to operate the two lasers in turn. To decrease the background noise, the time constant of a LIA was set to 10 ms, corresponding to the detection bandwidth of 25 Hz. The gas mixture of 5% $CO_2$:$N_2$ containing 4150 ppm water vapor at atmospheric pressure was introduced to the Double AmR #1. The period of each pulse ramp was set to 1 s with a duty cycle of 45.5%, which results in a scan rate of 3.5 $cm^{-1}/s$ and 2.6 $cm^{-1}/s$ for DL2 and DL1 lasers, respectively. The trailing edge of the waveform produced by the logical OR operation of the two pulse ramps triggered the range switch of the LIA since the $H_2O$ signal is ~10 times stronger than the $CO_2$ signal. A short interval of ~50 ms between the two adjacent pulse ramps from two channels of the AFG was implemented for the LIA setup time after the range switch. The spectral data and the pulse ramp signals are shown in Fig. 5. The complete 2f spectra of $H_2O$ and $CO_2$ were mapped every 1 s.

We demonstrated the optical signal addition and a two-gas rapid spectral measurement with a response time of 5 ms using a double AmR spectrophone. Performing a two spectra signal cancellation with the line-locked mode of two lasers at a specific concentration ratio of two target gases, the double AmR spectrophone measures directly the deviation of the concentration ratio. The deviation can then be used as a feedback to control gas valves to maintain a specific gas mixing ratio, which is important for controlling gas chemical reactions, gas mixtures or optimizing combustion processes.

This research was funded by the 973 program (grant 2012CB921603), the National Natural Science Foundation of China (grants 61275213, 61108030, 61127017, 61178009, 61378047, and 61205216), the National Key Technology R&D Program (2013BAC14B01), the Shanxi Natural Science Foundation (grants 2013021004-1 and 2012021022-1), the Shanxi Patent Promotion and Implementation Project, and the Shanxi Scholarship Council of China (2013-011, 2013-01).

## References

1. A. Miklós, P. Hess, and Z. Bozóki, Rev. Sci. Instrum. **72**, 1937 (2001).
2. J. P. Besson, S. Schilt, and L. Thévenaz, Spectrochim. Acta A **63**, 899 (2006).
3. Q. Y. Lu, Y. Bai, N. Bandyopadhyay, S. Slivken, and M. Razeghi, Appl. Phys. Lett. **97**, 231119 (2010).
4. Y. Ma, R. Lewicki, M. Razeghi, and F. K. Tittel, Opt. Express **21**, 1008 (2013).
5. M. E. Webber, M. Pushkarsky, and C. K. N. Patel, Appl. Opt. **42**, 2119 (2003).
6. A. A. Kosterev, Y. A. Bakhirkin, R. F. Curl, and F. K. Tittel, Opt. Lett. **27**, 1902 (2002).
7. M. Köhring, S. Böttger, U. Willer, and W. Schade, Opt. Express **21**, 20911 (2013).
8. K. Liu, X. Guo, H. Yi, W. Chen, W. Zhang, and X. Gao, Opt. Lett. **34**, 1594 (2009).
9. A. A. Kosterev and F. K. Tittel, Appl. Opt. **43**, 6213 (2004).
10. V. Spagnolo, L. Dong, A. A. Kosterev, D. Thomazy, J. H. Doty III, and F. K. Tittel, Appl. Phys. B **103**, 735 (2011).
11. L. Dong, J. Wright, B. Peters, B. A. Ferguson, F. K. Tittel, and S. McWhorter, Appl. Phys. B **107**, 459 (2012).
12. A. A. Kosterev, L. Dong, D. Thomazy, F. K. Tittel, and S. Overby, Appl. Phys. B **101**, 649 (2010).
13. V. Spagnolo, P. Patimisco, S. Borri, G. Scamarcio, B. E. Bernacki, and J. Kriesel, Opt. Lett. **37**, 4461 (2012).
14. A. A. Kosterev, P. R. Buerki, L. Dong, M. Reed, T. Day, and F. K. Tittel, Appl. Phys. B **100**, 173 (2010).
15. L. Dong, A. A. Kosterev, D. Thomazy, and F. K. Tittel, Appl. Phys. B **100**, 627 (2010).
16. K. Liu, H. Yi, A. A. Kosterev, W. Chen, L. Dong, L. Wang, T. Tan, W. Zheng, F. K. Tittel, and X. Gao, Rev. Sci. Instrum. **81**, 103103 (2010).
17. H. Yi, W. Chen, S. Sun, K. Liu, T. Tan, and X. Gao, Opt. Express **20**, 9187 (2012).
18. N. Petra, J. Zweck, A. A. Kosterev, S. E. Minkoff, and D. Thomazy, Appl. Phys. B **94**, 673 (2009).
19. L. Dong, V. Spagnolo, R. Lewicki, and F. K. Tittel, Opt. Express **19**, 24037 (2011).